Geoscience Frontiers xxx (2017) 1–12

HOSTED BY

ELSEVIER

Contents lists available at ScienceDirect

China University of Geosciences (Beijing)

Geoscience Frontiers

journal homepage: www.elsevier.com/locate/gsf

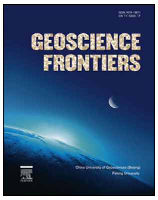

Research paper

New insights into petrogenesis of Miocene magmatism associated with porphyry copper deposits of the Andean Pampean flat slab, Argentina

Silvia I. Carrasquero [a], Nora A. Rubinstein [b,*], Anabel L.R. Gómez [b], Massimo Chiaradia [c], Dénis Fontignie [c], Victor A. Valencia [d]

[a] Facultad de Ciencias Naturales y Museo, Universidad Nacional de La Plata, La Plata, Argentina
[b] Instituto de Geociencias básicas, aplicadas y ambientales de Buenos Aires (IgeBA), Departamento de Ciencias Geológicas, Facultad de Ciencias Exactas y Naturales, Universidad de Buenos-CONICET, Argentina
[c] Department of Earth Sciences, University of Geneva, Switzerland
[d] School of Earth and Environmental Sciences Faculty, Washington State University, USA

ARTICLE INFO

Article history:
Received 28 October 2016
Received in revised form
16 August 2017
Accepted 5 October 2017
Available online xxx
Handling Editor: S. Ganguly

Keywords:
Porphyry copper deposits
Petrogenesis
Adakitic signal
Backarc
Central Andes

ABSTRACT

The Paramillos de Uspallata mining district located in the backarc region of the Pampean flat-slab segment (28°–33°S) features porphyry-type deposits genetically associated with Middle Miocene volcanics. This mineralizing magmatism comprising hydrothermally altered (sodic-calcic, potassic and phyllic alteration) subvolcanic and pyroclastic rocks of andesite-basaltic andesite and dacite-rhyolite composition with a typical arc signature, represents the eastward broadening of the Farellones arc by ∼17 Ma. Its geochemistry also reveals a residual mineralogy of amphibole ± garnet with limited plagioclase fractionation resulting in an adakitic signal; however, according to the isotopic data collected in our study, the contributions of MASH (melting-assimilation-storage-homogenization) processes in the acquisition of this signal cannot be disregarded.

Both the broadening of the Farellones arc and its residual mineralogy – typical of relatively deep magmatic chambers – are consistent with a slab shallowing and outcoming crustal thickening setting. This tectonic scenario could be interpreted as a result of an early effect of the Juan Fernandez Ridge collision that was further to the north by ∼17 Ma. Our findings suggest that magmas were fertile for porphyry type deposits during the early stages of the slab shallowing.

© 2017, China University of Geosciences (Beijing) and Peking University. Production and hosting by Elsevier B.V. This is an open access article under the CC BY-NC-ND license (http://creativecommons.org/licenses/by-nc-nd/4.0/).

1. Introduction

The flat-slab Pampean segment of the Central Andes of Argentina and Chile extends between 28° and 33°S (Fig. 1a) and is characterized by the lack of active volcanism and an intensive seismic activity (Barazangi and Isacks, 1976; Jordan et al., 1983). The shallowing of the subducting plate is tied to the collision of the Juan Fernandez Ridge (JFR) which began before 22 Ma in the northern part of the flat-slab segment and moved southeast reaching 33°S latitude at about 11 Ma (Yáñez et al., 2001). By ∼20 Ma the Principal Cordillera was not affected by the collision of the JFR at 32°–33°S latitude and the Farellones volcanic arc was active along its Chilean slope up to 16 Ma (Rivano et al., 1990). Deformation at that time was constrained to the axis of the Cordillera and to the western part of the Aconcagua fold and thrust belt whereas the back-arc still remained undeformed (Ramos et al., 2002). In the Paramillos back-arc region, an andesitic magmatism probably associated with a second slab dehydration front, occurred between ∼20 and 16 Ma coevally with the Farellones arc (Ramos et al., 2002). Owing to the onset of the slab flattening, at ∼15 Ma the volcanic front shifted 50 km to the east of the Farellones arc after the eastward migration of the orogenic front to the Frontal Cordillera, remaining active from ∼15 to 9 Ma (Ramos et al., 2002). The geochemical features of these magmas changed from calcoalcaline to adakitic reflecting the progressive crustal thickening beneath the arc (Kay and Mpodozis, 2002). By ∼9 Ma, 2 Ma later

---

[*] Corresponding author.
E-mail address: nora@gl.fcen.uba.ar (N.A. Rubinstein).
Peer-review under responsibility of China University of Geosciences (Beijing).

https://doi.org/10.1016/j.gsf.2017.10.009

1674-9871/© 2017, China University of Geosciences (Beijing) and Peking University. Production and hosting by Elsevier B.V. This is an open access article under the CC BY-NC-ND license (http://creativecommons.org/licenses/by-nc-nd/4.0/).

Please cite this article in press as: Carrasquero, S.I., et al., New insights into petrogenesis of Miocene magmatism associated with porphyry copper deposits of the Andean Pampean flat slab, Argentina, Geoscience Frontiers (2017), https://doi.org/10.1016/j.gsf.2017.10.009

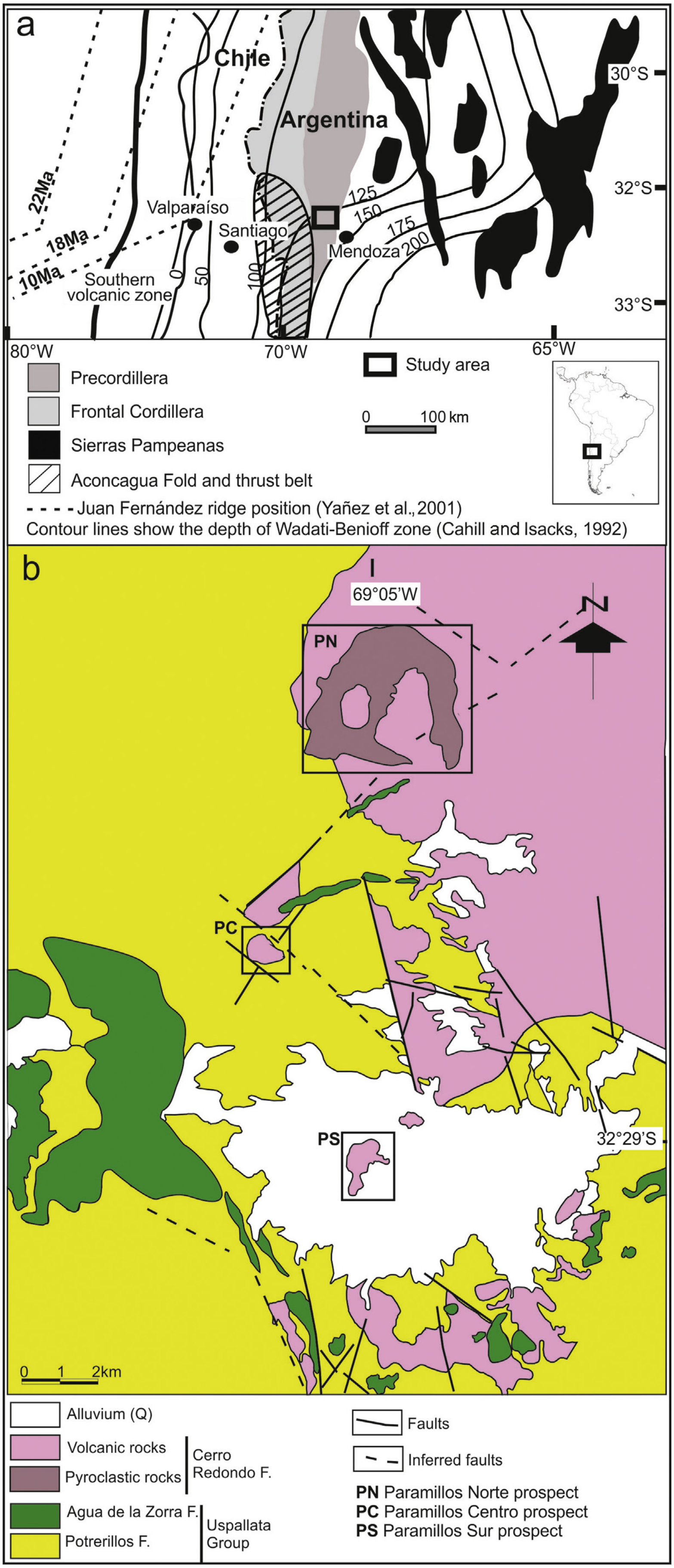
a
Chile
Argentina
30°S
32°S
33°S
22Ma
18Ma
10Ma
Valparaíso
Santiago
Mendoza
Southern volcanic zone
0
50
100
125
150
175
200
80°W
70°W
65°W
Study area
0 100 km
Precordillera
Frontal Cordillera
Sierras Pampeanas
Aconcagua Fold and thrust belt
Juan Fernández ridge position (Yañez et al., 2001)
Contour lines show the depth of Wadati-Benioff zone (Cahill and Isacks, 1992)
b
69°05'W
N
PN
PC
PS
32°29'S
0 1 2km
Alluvium (Q)
Volcanic rocks
Pyroclastic rocks
Cerro Redondo F.
Agua de la Zorra F.
Potrerillos F.
Uspallata Group
Faults
Inferred faults
PN Paramillos Norte prospect
PC Paramillos Centro prospect
PS Paramillos Sur prospect

Please cite this article in press as: Carrasquero, S.I., et al., New insights into petrogenesis of Miocene magmatism associated with porphyry copper deposits of the Andean Pampean flat slab, Argentina, Geoscience Frontiers (2017), https://doi.org/10.1016/j.gsf.2017.10.009

than the collision of the JFR at that latitude, deformation shifted to the western Precordillera at high propagation rate as a result of a peak of the shallowing. The magmatic activity, typically high K to shoshonitic, concentrated further to the east in the Sierras Pampeanas back-arc region between 8 and 5 Ma and ended completely at ~2 Ma (Kay and Mpodozis, 2002; Ramos et al., 2002).

The word adakite introduced by Defant and Drummond (1990) refers to intermediate to acidic plutonic and volcanic rocks which appear to be products of direct partial melting of subducted oceanic lithosphere at high pressure in which garnet is a stable residual phase and plagioclase is absent (Peacock et al., 1994; Martin, 1999). According to Peacock et al. (1994) the necessary geodynamic condition which allows for the formation of adakitic magmas is the subduction of young and hot oceanic plates. More recently, other authors have proposed that adakitic rocks can be generated in the presence of asthenospheric window (Yogodzinski et al., 2001), partial melting of thickened lower crust (e.g. Atherton and Petford, 1993; Petford and Atherton, 1996), high pressure fractionation of garnet and amphibole (Muntener et al., 2001; Alonso-Perez et al., 2009; Chiaradia, 2015 and references therein) or delaminated mafic lower crust (e.g. Defant et al., 2002; Xu et al., 2002). However, key adakitic geochemical features can be produced in normal asthenosphere derived arc magmas by melting-assimilation-storage-homogenization (MASH) and assimilation-fractional-crystallization (AFC) processes (Richards and Kerrich, 2007) which have been well documented particularly in the Central Andes (López Escobar, 1982; Kay et al., 1987, 1991; Hildreth and Moorbath, 1988).

Porphyry copper deposits are mineralized magmatic-hydrothermal systems which at present constitute the main primary source of Cu supply in the world. These deposits are closely linked to their geodynamic setting and usually associated with calc-alkaline and adakitic magmatism in subduction zones (Cline and Bodnar, 1991; Thiéblemont et al., 1997; Oyarzún et al., 2001; Rabbia et al., 2002; Reich et al., 2003; Richards and Kerrich, 2007; Chiaradia et al., 2012). It is now widely accepted that these deposits result from a dual melting process which included not only an initial melting in the metasomatized mantle wedge, above the subducting oceanic slab, yielding relatively oxidized and sulfur-rich mafic magmas with incompatible chalcophile or siderophile elements (such as Cu or Au) but also a secondary melting by injection of dykes and sills in the MASH zone of the lower crust, yielding a crustal and mantle-derived hybrid magma, with a high content of volatile and metalliferous elements and density low enough to allow its upward migration to occur (Richards, 2003, 2011).

In this paper, we present new geochemical, geochronological and isotopic data of magmatic rocks genetically associated with porphyry copper deposits in the Paramillos de Uspallata mining district located in the southern part of the Pampean flat slab segment. Our aim is to integrate this petrological information into a possible petrogenetic framework, as not enough data has yet been collected for regional-scale studies of magmatism precursor of porphyry type deposits.

2. Regional geological setting

The Paramillos de Uspallata mining district (32°29′–32°25′S; 69°5′–69°7′W) is located in the southern part of the Argentine Precordillera fold and thrust belt (Fig. 1a and b). The oldest rocks of this part of the Precordillera are Middle Devonian clastic sedimentites of submarine fans deposits (Harrington, 1971) metamorphosed and successively deformed by the Late Devonian Famatinian Orogeny resulting from the collision of the Chilenia terrane (Ramos et al., 1986) and the Early Permian San Rafael Orogeny (Cortés et al., 1997). These low grade metamorphic rocks are overlain by Upper Permian volcanic and pyroclastic rocks mainly of rhyolitic-dacitic composition (Cortés et al., 1997) resulting from the end of the Lower Permian subduction and the extensional collapse of the orogen at the western margin of the Gondwanaland (Kleiman and Japas, 2009) which ends with Cuyo rift basin formation (Legarreta and Uliana, 1996).

The infilling of the Cuyo basin consists of up to 3700 m of a volcano-sedimentary sequence overlying the Paleozoic basement. Its lower part includes sandstones, shales, mudstones and tuffs (Potrerillos and Agua de la Zorra Formations, see Fig. 1b) of fluvial, lacustrine and deltaic environment with episodic eruptive events deposited during the Early to Mid-Triassic synrift stage characterized by tectonic subsidence (Spalletti, 1999). Tholeiitic to slightly alkaline lava flows and minor sills basalts emplaced during the Middle Triassic (~235 Ma) in this synrift phase (Massabie, 1986; Ramos and Kay, 1991). These deposits were overlaid by Middle to Early Late Triassic dominant fluvial-lacustrine successions deposited under thermal-tectonic subsidence (sag phase) conditions of the basin. Likewise, its upper part consists of Late Triassic alluvial-fluvial successions related to tectonic subsidence reactivation. Thermal relaxation of the basin finished with the flexural subsidence of the lithosphere triggered by the Andean Orogeny during the Cenozoic (Spalletti, 1999; Barredo et al., 2012).

During the Miocene (~19 to 16 Ma) an arc magmatism produced a large volume of subvolcanic rocks (Massabie et al., 1986; Kay et al., 1991) folded by the Andean Orogeny (Cerro Redondo Formation, see Fig. 1b). At regional scale these subvolcanics are mainly sills of phenodacitic to phenoandesitic composition with biotite and amphibole and variable propilititic alteration (Cortés et al., 1997).

3. Miocene magmatism and mineralization of the Paramillos de Uspallata mining district

This mining district includes three porphyry-type deposits spatially associated with Miocene magmatism of the area (Paramillos Norte, Paramillos Centro and Paramillos Sur, Fig. 1b) explored in the 1960s by a state-owned exploration company (*Dirección General de Fabricaciones Militares*). The exploration program encompassed regional geological mapping, surface and drill geochemical sampling (analyzing Cu, Mo, Pb and Zn), inductive polarization studies and a total of 8650 m of drilling (Lavandaio and Fusari, 1999; Romani, 1999 and references therein).

3.1. Miocene magmatism

The Miocene magmatism of the study area includes subvolcanic and minor pyroclastic rocks. The pyroclastic rocks correspond to welded massive tuffs variably affected by hydrothermal alteration which consist of plagioclase and amphibole crystals, oriented *fiammes* and minor volcanic and slate fragments in an aphanitic matrix. Microscopically, they show porphyroclastic texture with plagioclase, quartz, and amphibole crystaloclasts and accessory titanite and magnetite along with plagioclase-phyric andesitic lithic fragments in a very fine-grained matrix where ghost-like impressions of flattened shards could be identified.

The subvolcanic rocks occur as small stocks and dikes intruding the pyroclastic rocks. They are mainly phenoandesites composed of plagioclase and amphibole phenocrysts enclosed in an aphanitic groundmass with variable sodic-calcic, potassic and phyllic

Figure 1. (a) Paramillos de Uspallata mining district location at the southern part of the Pampean flat slab segment in the Southern Central Andes showing the position of the JFR at 22 Ma (solid line), 18 Ma (fine dotted line) and 10 Ma (dash line). Gray solid lines show the depth of the subducted slab; (b) simplified geological map and location of the porphyry type deposits of the Paramillos de Uspallata mining district area.

Please cite this article in press as: Carrasquero, S.I., et al., New insights into petrogenesis of Miocene magmatism associated with porphyry copper deposits of the Andean Pampean flat slab, Argentina, Geoscience Frontiers (2017), https://doi.org/10.1016/j.gsf.2017.10.009

alteration. Microscopically, they show plagioclase, amphibole, augite and scarce biotite and K-feldspar phenocrysts in a fine-grained plagioclase groundmass; the accessory minerals consist of apatite, magnetite, titanite and zircon. Scarce small and wormy propylitized trachyandesitic dikes intrude the andesites. They have fine-grained texture and consist of K-feldspar, subordinate plagioclase and minor quartz frequently with poikilomosaic texture.

3.2. *Porphyry type deposits*

3.2.1. *Paramillos Sur*

This prospect, with mineral resource of 186 Mt of 0.58%–0.95% Cu and 0.07% Mo (Romani, 1999), is hosted by andesitic subvolcanic rocks affected by an alteration halo of ~0.25 km^2 (Figs. 1b and 2a) consisting of a potassic alteration core irregularly surrounded by a phyllic zone. The potassic alteration is moderate to strong and occurs pervasively and in veinlets. The pervasive assemblage consists of K-feldspar, biotite, magnetite and quartz (Fig. 2b). Veinlets up to 1 cm thick are frequent in this alteration zone and are composed of quartz, K-Feldspar + biotite + quartz + chalcopyrite ± bornite. The phyllic halo partially overprints the potassic alteration. It shows a moderate pervasive sericitization and a strong veinlet-type silicification along with disseminated pyrite. It is moderately oxidized with Fe-oxides, jarosite and scarce malachite. A late weak pervasive carbonatization overprints both the potassic and phyllic alteration. K–Ar whole rock dating of two drill samples with potassic overprinted by phyllic alteration yielded ages of 15.2 ± 0.5 and 15.8 ± 1 Ma (Koukharsky et al., 1998).

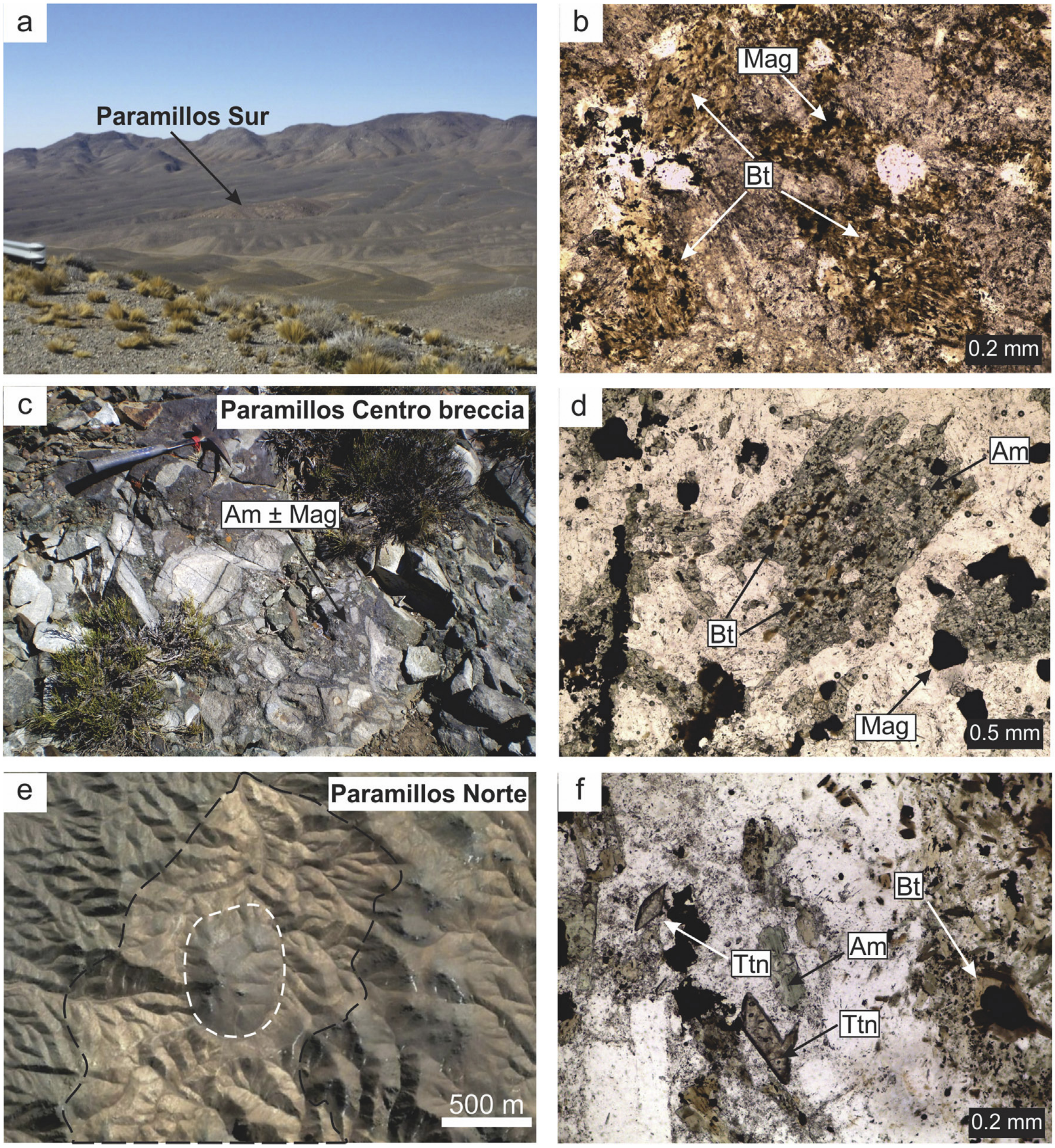

Figure 2. (a) Panoramic view of the Paramillos Sur alteration halo; (b) microphotograph showing Paramillos Sur andesite with pervasive potassic alteration with biotite (Bt) and magnetite (Mag) (transmitted light with PPL = plane polarized light); (c) breccia with magnetite + fibrous amphibole (Am) cement in Paramillos Centro prospect; (d) microphotograph showing Paramillos Centro andesite with pervasive sodic-calcic alteration (fibrous amphiboles and magnetite) with overprinting of biotite (transmitted light with PPL); (e) Google earth image of the Paramillos Norte alteration halo showing the sodic-calcic core (white dotted line) surrounded by the phyllic zone (black dotted line); (f) microphotograph showing Paramillos Norte andesite with pervasive sodic-calcic alteration composed by fibrous amphiboles and titanite (Ttn) with overprinting of biotite (transmitted light with PPL).

Please cite this article in press as: Carrasquero, S.I., et al., New insights into petrogenesis of Miocene magmatism associated with porphyry copper deposits of the Andean Pampean flat slab, Argentina, Geoscience Frontiers (2017), https://doi.org/10.1016/j.gsf.2017.10.009

3.2.2. Paramillos Centro

This prospect (Fig. 1b), with no available mineral resource data, is hosted by a small andesitic subvolcanic outcrop affected by sodic-calcic, potassic and phyllic alteration. The sodic-calcic alteration is weak and occurs mainly pervasively and also as breccia cement and in veinlets up to 10 mm thick (Fig. 2c). The alteration assemblage consists of fibrous amphibole and minor carbonate, epidoto, titanite and chlorite along with abundant disseminated magnetite (Fig. 2d). Overprinting the sodic-calcic halo there is a weak pervasive potassic alteration with an assemblage of K-feldspar and biotite. Partially surrounding this halo and overprinting the potassic alteration, there is a phyllic halo with moderate to strong pervasive silicification and sericitization and disseminated pyrite crystals. Scarce veinlets up to 5 mm thick composed of quartz or pyrite are locally recognized. This phyllic zone is moderately to strongly oxidized with Fe-oxides and less abundant jarosite.

3.2.3. Paramillos Norte

Although there is no information on this prospect mineral resources, drill geochemical exploration returned ore grades up to 1.7% Cu and 0.07% Mo (Lavandaio and Fusari, 1999). The deposit is hosted by andesitic subvolcanics intruding pyroclastic rocks affected by an alteration halo of ~15 km^2 (Figs. 1b and 2e). The core shows a weak to moderate sodic-calcic alteration affecting the andesites. The pervasive assemblage consists mainly of magnetite and fibrous amphibole with minor titanite and epidote and scarce carbonate. Magnetite ± fibrous amphibole veinlets with wormy walls and up to 100 mm thick are frequent and locally they form breccia zones. Weak to moderate pervasive and rarely veinlet-type feldspatization and biotitization are irregularly distributed in this alteration zone with the biotite replacing the fibrous amphibole (Fig. 2f). Scarce veinlets with straight wall up to 3 cm thickness composed of magnetite or magnetite + quartz are locally observed. Surrounding the core, there is a phyllic halo developed in the pyroclastic rocks and partially overprinting the sodic-calcic and potassic alteration. It shows weak to moderate pervasive sericitization and silicification with disseminated pyrite crystals along with moderate amount of quartz ± pyrite and pyrite veinlets up to 20 mm thick. This phyllic zone is moderately to strongly oxidized with abundant jarosite and minor Fe-oxides. K–Ar dating of a muscovite concentrate yielded an age of 16.0 ± 0.3 Ma for the hydrothermal system (Sillitoe, 1977). Trachyandesitic dikes weakly altered to calcite and minor epidote intrude the andesites with the carbonatization extending into the host subvolcanics.

4. Methods and analytical procedures

Due to the hydrothermal alteration affecting the sampled areas, careful selection of the least altered material present was carried out during the sampling, whenever possible. A detailed petrographic study of the alteration assemblages was performed in order to achieve robust geochemical interpretations. 12 rock samples were analyzed for major and trace elements at the University of Lausanne (Switzerland) by X-ray fluorescence (XRF) and Activation Laboratories (Actlabs) by Instrumental Neutron Activation Analysis (INAA). XRF analyses were performed using a Philips PW 2400 diffractometer with Rh anode and detection limits of 0.01% for major elements and 5 ppm for traces. INAA analyses were performed following the method proposed by Hoffman (1992). Samples and an internal standard are irradiated with a thermal neutron flux of 7×10^{12} $n\ cm^{-2}\ s^{-1}$. The samples are counted on a high purity Ge detector with resolution of better than 1.7 keV. The decay-corrected activities are compared to a calibration developed from multiple reference materials. Five rock samples were analyzed for major and trace elements at Actlabs by inductively coupled plasma/mass spectrometry (ICP/MS, code 4LithoResearch) with a Perkin Elmer Sciex ELAN 6000, 6100 or 9000 spectrometer.

Five surface whole-rocks were analyzed for Sr, Nd and Pb isotopes at the Department of Mineralogy, University of Geneva, using a mass spectrometer. Pb was loaded onto Re filaments using the silica gel technique and all samples (and standards) were measured at 1220 °C. Pb isotope ratios were corrected for instrumental fractionation by a factor of 0.07% per a.m.u. based on more than 90 measurements of the SRM981 standard (Todt et al., 1984). External reproducibility of the standard ratios is 0.11% for $^{206}Pb/^{204}Pb$, 0.12% for $^{207}Pb/^{204}Pb$ and 0.20% for $^{208}Pb/^{204}Pb$. Sr was loaded on single Re filaments with a Ta oxide solution and measured at 1480 °C. $^{87}Sr/^{86}Sr$ values were internally corrected for fractionation using an $^{88}Sr/^{86}Sr$ value of 8.375209. Raw values were further corrected for external fractionation by a value of +0.03‰, determined by repeated measurements of the SRM987 standard ($^{87}Sr/^{86}Sr = 0.710250$). External reproducibility of the $^{87}Sr/^{86}Sr$ ratio for the SRM987 is 7 ppm. Nd was loaded onto double Re filaments with 1 M HNO_3. $^{143}Nd/^{144}Nd$ values were internally corrected for fractionation using a $^{146}Nd/^{144}Nd$ value of 0.7219 and the ^{144}Sm interference on ^{144}Nd was monitored on the mass ^{147}Sm and corrected using a $^{144}Sm/^{147}Sm$ value of 0.206700. External reproducibility of the JNdi-1 standard (Tanaka et al., 2000) is 55 ppm.

One andesite surface sample was selected for zircon U/Pb dating. Heavy mineral concentrates of the <350 μm fraction were separated using traditional techniques at ZirChron LLC. Laser Ablation Inductively Coupled Plasma Mass Spectrometry (LA-ICP-MS) U/Pb analyses were conducted at Washington State University prior to cathodoluminescence imaging using a New Wave NdYAG UV 213-nm laser coupled to a 2-single collector, double-focusing, magnetic sector ICP-MS. Operating procedures and parameters are a slight modification of Chang et al. (2006). Laser spot size and repetition rate were 30 m and 10 Hz, respectively. Two zircon standards were used: Plesovice (Sláma et al., 2008) and FC-1 (Paces and Miller, 1993). U–Pb ages were calculated using Isoplot (Ludwig, 2003). U–Pb zircon crystallization age errors are reported using quadratic sum of the weighted mean error plus the total systematic error for the set of analyses (Valencia et al., 2005).

5. Results

5.1. U–Pb geochronology

Zircon crystals from sample 87190 show mainly euhedral morphologies and low U/Th ratios consistent with magmatic origin (Rubatto, 2002). A total of 41 zircons were analyzed (Table 1) which yielded an $^{206}Pb/^{238}U$ age of 16.9 ± 0.3 Ma ($n = 35$, 2σ) with an inherited age of ~237 Ma (Fig. 3) approximately corresponding to the Middle Triassic ages obtained for the pyroclastic levels intercalated within the fluvial deposits of the Potrerillos Formation (Uspallata Group) elsewhere in the Cuyo Basin (Spalletti et al., 2008).

5.2. Major and trace element composition

Chemical analyses and hydrothermal alteration type of representative samples of the Miocene igneous rocks from the Paramillos area are shown in Table 2. It is essential to consider

Please cite this article in press as: Carrasquero, S.I., et al., New insights into petrogenesis of Miocene magmatism associated with porphyry copper deposits of the Andean Pampean flat slab, Argentina, Geoscience Frontiers (2017), https://doi.org/10.1016/j.gsf.2017.10.009

hydrothermal alteration in the interpretation of rocks geochemistry as it is generally accepted that mobility of large ion lithophile elements (LILE) and, to a lesser extent, light rare earth elements (LREE) is strongly affected, whereas high field strength elements (HFSE) and mid- to heavy rare earth elements (MREE, HREE) almost behave as immobile (e.g., Rollinson, 1995; Kay et al., 2005). Bearing this in mind, the Nb/Y versus Zr/TiO_2 diagram of Pearce (1996) was used to classify the analyzed rocks. According to this classification (Fig. 4a), these rocks are rhyodacite-dacite, andesite-basaltic andesite and minor trachy-andesite with a narrow range of SiO_2 (56.78–64.29 wt.%) and variable Na_2O (3.05–7.09 wt.%), K_2O (0.4–10.09 wt.%) and Al_2O_3 (17.49–21.65 wt.%) in free-basis. High K_2O contents correspond to samples bearing noticeable potassic alteration (Table 2). Besides, these rocks show a metaluminous character except for those affected by phyllic alteration which are markedly peraluminous (Fig. 4b and Table 2).

The N-MORB normalized trace element pattern of the analyzed rocks is similar to that of other unaltered Miocene rocks of the area (Fig. 5a). It shows a strong relative enrichment in LILE, a Nb trough and negative anomalies in P and Ti which are common features of calc-alkaline arc magmas. Ba/La ratios (Table 2) confirm a volcanic arc affinity (Ba/La >20) except for Paramillos Sur samples, in which the low Ba/La could be attributed to the high mobility of the Ba during the phyllic alteration. Regarding REE pattern (Fig. 5b), it is slightly more depleted in HREE (La/Yb up to 39) than the unaltered Miocene rocks of the area (La/Yb up to 20.68) and displays slightly negative to positive Eu anomalies (Eu/*Eu: 0.76–1.44, calculated using the software Petrograph) along with a flat pattern in the MREE-HREE, indicative of amphibole ± garnet fractionation. Moreover, the slightly negative to positive Eu anomalies together with an increase of the La/Yb ratios coupled with low La/Sr ratios (Fig. 6a) suggest a lesser role of plagioclase as a residual mineral (see Kay et al., 1991). Besides, the Paramillos volcanics show a trend from the normal arc magmas field toward the adakitic field (Fig. 6b).

5.3. Sr–Nd–Pb isotope compositions

The Sr–Nd isotope ratios, that were corrected for the obtained age of 16.9 Ma, display a wide range of $(^{87}Sr/^{86}Sr)_T$ (0.7040–0.7056) and $(^{143}Nd/^{144}Nd)_T$ (0.5125–0.5128) ratios (Table 3; Fig. 7a). Furthermore, the Pb isotope ratios (Table 3) display a wide range of $^{206}Pb/^{204}Pb$ (18.4732–18.7841), $^{207}Pb/^{204}Pb$ (15.5865–15.6309) and $^{208}Pb/^{204}Pb$ (38.2557–38.5662) values.

In the $^{143}Nd/^{144}Nd$ versus $^{87}Sr/^{86}Sr$ diagram (Fig. 7a), the analyzed rocks plot in the Mantle Array showing a well-defined

Table 1
U/Pb isotopic data for zircons crystal from sample 87190 obtained by LA-ICPMS.

Sample 87190	U (ppm)	Th/U	$^{238}U/^{206}Pb$	1σ % error	$^{207}Pb/^{206}Pb$	σ % error	$^{206}Pb/^{238}U$ age (Ma)	1σ abs err	$^{207}Pb/^{206}Pb$ age (Ma)	1σ abs err	Best age (Ma)	1σ abs err Ma
Z_58	277	0.84	385.5555	2.59%	0.0476	3.73%	16.7	0.4	79.4	86.2	16.7	0.4
Z_57	237	0.81	388.3576	2.72%	0.0520	3.65%	16.6	0.5	286.7	81.3	16.6	0.5
Z_56	317	0.80	392.3876	2.41%	0.0492	3.73%	16.4	0.4	156.6	85.1	16.4	0.4
Z_55	373	0.44	376.7915	2.32%	0.0509	3.44%	17.1	0.4	236.7	77.4	17.1	0.4
Z_54	485	0.97	385.4178	2.07%	0.0465	3.15%	16.7	0.3	21.4	74.0	16.7	0.3
Z_53	1785	1.70	387.1356	3.95%	0.0520	5.69%	16.6	0.7	287.3	125.2	16.6	0.7
Z_4	176	0.46	371.0453	2.61%	0.0470	4.33%	17.4	0.5	47.9	100.3	17.4	0.5
Z_52	123	0.46	380.8477	3.69%	0.0535	5.12%	16.9	0.6	350.1	111.9	16.9	0.6
Z_50	136	0.75	393.7187	3.60%	0.0512	4.18%	16.4	0.6	248.4	93.4	16.4	0.6
Z_49	121	0.67	379.7621	3.81%	0.0576	4.66%	17.0	0.6	515.5	99.2	17.0	0.6
Z_47	132	0.49	376.2556	3.34%	0.0531	4.46%	17.1	0.6	334.1	98.0	17.1	0.6
Z_46	242	1.03	388.7004	2.72%	0.0475	3.69%	16.6	0.5	74.4	85.4	16.6	0.5
Z_45	136	0.59	386.5538	3.46%	0.0487	4.72%	16.7	0.6	131.1	107.4	16.7	0.6
Z_44	1625	1.75	27.0792	2.25%	0.0510	0.63%	233.8	5.2	239.2	14.5	233.8	5.2
Z_43	89	0.51	392.3670	5.07%	0.0536	5.62%	16.4	0.8	352.9	122.2	16.4	0.8
Z_42	88	0.72	384.6847	4.50%	0.0714	4.82%	16.7	0.8	968.6	95.4	16.7	0.8
Z_41	108	0.56	388.5341	4.22%	0.0530	4.58%	16.6	0.7	330.3	100.7	16.6	0.7
Z_40	128	0.46	374.7058	3.72%	0.0438	4.42%	17.2	0.6	0.0	0.0	17.2	0.6
Z_39	82	0.56	376.1209	4.62%	0.0532	5.60%	17.1	0.8	335.9	122.2	17.1	0.8
Z_38	118	0.50	366.9291	3.23%	0.0590	4.54%	17.5	0.6	568.1	95.8	17.5	0.6
Z_34	538	0.45	26.6729	1.90%	0.0510	0.74%	237.3	4.4	240.8	16.9	237.3	4.4
Z_32	189	0.80	374.6185	2.84%	0.0501	4.47%	17.2	0.5	200.0	100.6	17.2	0.5
Z_27	342	0.93	379.0173	2.90%	0.0535	3.50%	17.0	0.5	349.9	77.3	17.0	0.5
Z_20	110	0.49	368.9618	3.57%	0.0532	5.01%	17.4	0.6	336.7	109.6	17.4	0.6
Z_26	116	0.78	388.2251	3.71%	0.0658	4.36%	16.6	0.6	801.0	88.8	16.6	0.6
Z_25	119	0.50	380.6593	4.19%	0.0570	5.04%	16.9	0.7	489.7	107.4	16.9	0.7
Z_24	166	0.89	380.3495	3.60%	0.0589	4.08%	16.9	0.6	565.0	86.5	16.9	0.6
Z_23	587	0.78	40.9357	2.76%	0.0521	1.62%	155.6	4.2	289.7	36.6	155.6	4.2
Z_22	301	0.75	382.9069	3.06%	0.0467	3.68%	16.8	0.5	33.8	85.9	16.8	0.5
Z_21	125	0.55	375.1998	3.33%	0.0554	4.43%	17.2	0.6	427.4	95.9	17.2	0.6
Z_19	286	0.82	371.4840	2.72%	0.0496	3.40%	17.3	0.5	174.1	77.5	17.3	0.5
Z_18	253	0.90	382.4825	2.10%	0.0507	3.66%	16.8	0.4	226.8	82.5	16.8	0.4
Z_17	160	0.68	394.4127	3.26%	0.0520	4.04%	16.3	0.5	286.4	89.9	16.3	0.5
Z_16	81	0.64	378.1152	4.13%	0.0619	5.87%	17.0	0.7	670.0	120.9	17.0	0.7
Z_15	1065	1.74	26.6861	1.14%	0.0513	0.98%	237.1	2.7	253.8	22.4	237.1	2.7
Z_14	932	1.34	26.3182	1.17%	0.0522	1.01%	240.4	2.8	292.2	22.9	240.4	2.8
Z_11	155	0.86	380.8373	3.10%	0.0492	4.51%	16.9	0.5	158.4	102.3	16.9	0.5
Z_10	477	1.76	368.6695	2.87%	0.0524	3.02%	17.5	0.5	304.9	67.5	17.5	0.5
Z_9	404	0.57	26.6577	1.40%	0.0507	1.17%	237.4	3.3	225.8	26.8	237.4	3.3
Z_8	122	0.84	368.9383	3.46%	0.0457	4.72%	17.4	0.6	0.0	92.8	17.4	0.6
Z_1	144	0.84	380.3805	3.30%	0.0468	4.59%	16.9	0.6	36.8	106.4	16.9	0.6

Please cite this article in press as: Carrasquero, S.I., et al., New insights into petrogenesis of Miocene magmatism associated with porphyry copper deposits of the Andean Pampean flat slab, Argentina, Geoscience Frontiers (2017), https://doi.org/10.1016/j.gsf.2017.10.009

array toward the enriched mantle (EMII), similarly to Miocene volcanics from elsewhere in the flat slab region of the Central Andes (Kay et al., 1991) and particularly with those genetically associated with porphyry copper deposits (e.g. Bissig et al., 2003; Reich et al., 2003). Additionally, these rocks plot in the lower continental crust field close to the EMII in the $^{207}Pb/^{204}Pb$ vs. $^{206}Pb/^{204}Pb$ diagram (Fig. 7b). These isotopic values could be interpreted as a mixing process between a mantle-derived component and a crustal component in their genesis. The inherited Triassic age, which coincides with the age of the synrift deposits of the Cuyo basin, suggests the involvement of an upper crust in this process.

6. Discussion

The new geochemical, geochronological and isotopic data of the Paramillos area magmatism presented herein provide new insights into the petrogenesis of the porphyry copper deposits.

Although Paramillos Miocene magmatism is located in a backarc position, the Ba/La ratios confirm a volcanic arc affinity. Moreover, this magmatism has some geochemical similarities with the coeval Farellones arc volcanics of the Aconcagua region (see Kay and Mpodozis, 2002 and references therein), suggesting an eastward broadening of this arc by ~17 Ma according to our geochronologic data. The middle Miocene expansion of arc volcanism is also recorded further to the south in the Payenia segment from ~18 Ma (Kay et al., 2006). In addition, magmatism age (16.9 ± 0.3 Ma) is very close to hydrothermal alteration age (16.0 ± 0.3 Ma; Sillitoe, 1977) in the Paramillos Norte deposit, proving mineralizing potential for the Middle Miocene magmatism which has not yet been well documented in literature.

Our geochemical results also reveal that this arc magmatism has an adakitic trend and a residual mineralogy of amphibole ± garnet with limited plagioclase fractionation. This chemical signature is typical of calc-alkalic magmatism precursor of porphyry copper deposits (Loucks, 2014) in which amphibole ± garnet fractionation occurs in the lower crust due to a combination of high water content, high pressure, and high oxidation state (e.g., Richards, 2011; Chiaradia et al., 2012).

According to Sillitoe (2010) there is an empirical relationship between the development of productive porphyry type deposits, broadly contractional settings with crustal thickening and rapid exhumation. Contractional conditions favor magma storage in large confined crustal chambers promoting an effective fractionation and fluid generation that could be released by decompression due to rapid exhumation (Sillitoe and Perelló, 2005) that may occur as a result of stress relaxation conditions at the end of an orogeny

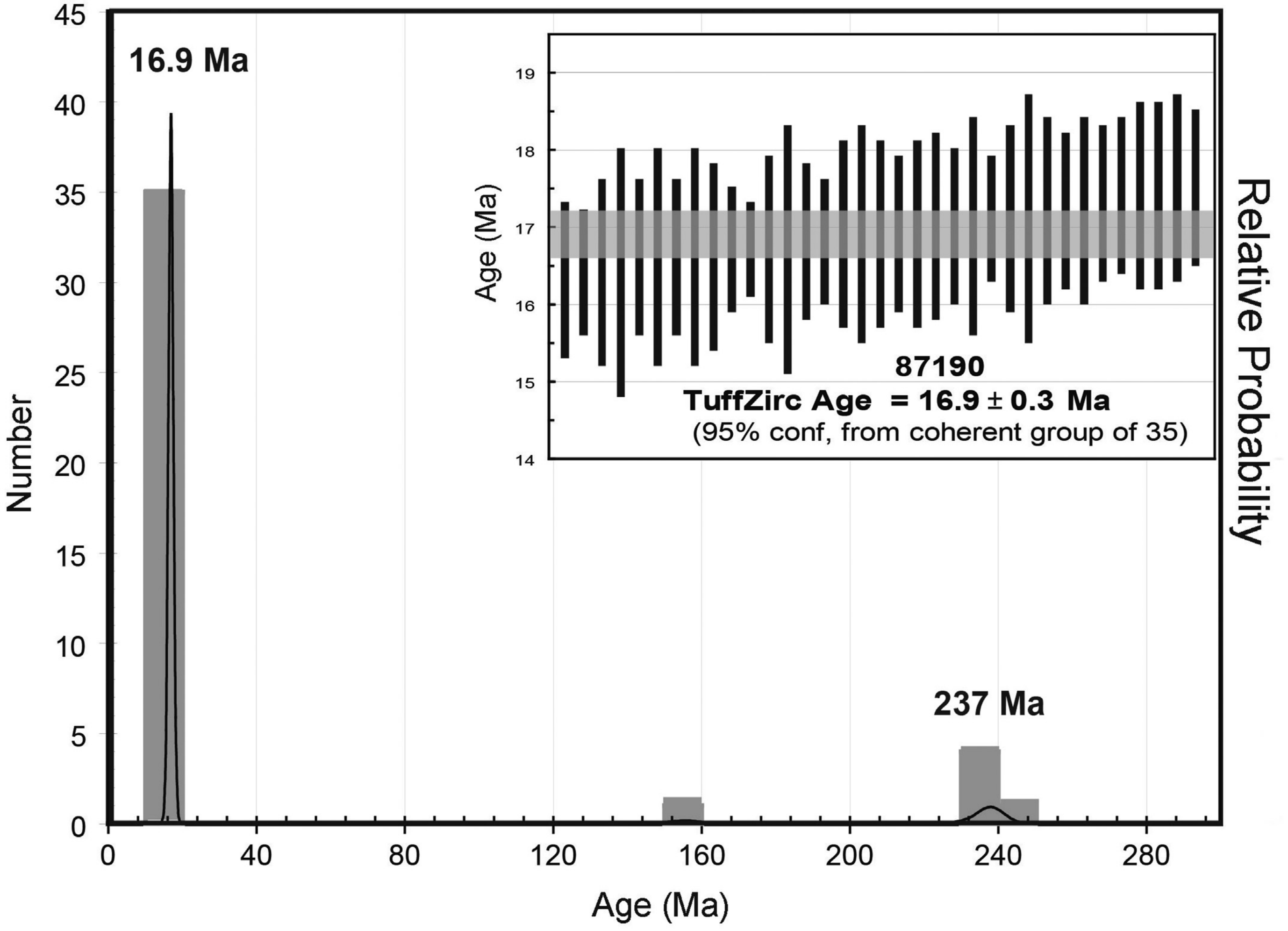

Figure 3. U–Pb zircon histogram and cumulative probability plots of LA-ICP-MS U–Pb zircon dating results.

Please cite this article in press as: Carrasquero, S.I., et al., New insights into petrogenesis of Miocene magmatism associated with porphyry copper deposits of the Andean Pampean flat slab, Argentina, Geoscience Frontiers (2017), https://doi.org/10.1016/j.gsf.2017.10.009

Table 2
Major (wt.%) and trace element (ppm) contents of Miocene volcanics from the study area. *Samples analyzed by ICP/MS (code 4LithoResearch), Actlabs.

Samples	UP79	UP82	UP84	UP85	87154*	87144*	87169*	87190*	87193*	UP52	UP54	UP69	UP72	UP73	UP74	Gn14	Gn15
Ore deposit	Paramillos Norte	Paramillos Norte	Paramillos Norte	Paramillos Norte	Paramillos Norte	Paramillos Norte	Paramillos Norte	Paramillos Norte	Paramillos Norte	Paramillos Centro	Paramillos Centro	Paramillos Centro	Paramillos Centro	Paramillos Centro	Paramillos Centro	Paramillos Sur	Paramillos Sur
Lithology	Traquitic Pyroclastite	Andesitic Pyroclastite	Traquiandesite Sub-volcanic	Rhyolite-dacite Sub-volcanic	Andesite Sub-volcanic	Traquiandesite Sub-volcanic	Rhyolite-dacite Sub-volcanic	Andesite Sub-volcanic	Andesite Sub-volcanic	Andesite Sub-volcanic	Andesite Sub-volcanic	Rhyolite-dacite Sub-volcanic	Rhyolite-dacite Sub-volcanic	Rhyolite-dacite Sub-volcanic	Andesite Sub-volcanic	Sub-volcanic	Sub-volcanic
Alteration Assemblage	Potassic, phyllic	Phyllic, Oxidation	Potassic, Phyllic and Oxidation	Potassic	Potassic	Potassic, Phyllic and Carbonatic	Sodic-calcic, Potassic	Sodic-calcic	Sodic-calcic	Sodic-calcic, Potassic	Sodic-calcic, Potassic	Sodic-calcic	Sodic-calcic, Potassic	Sodic-calcic	Sodic-calcic, Potassic,	Potassic, Phyllic	Potassic, Phyllic
Alteration intensity	Moderate	Moderate	Weak to moderate	Weak to moderate	Weak to moderate	Weak	Weak	Weak to moderate	Weak to moderate	Moderate	Moderate	Moderate	Weak to moderate	Weak to moderate	Weak to moderate	Moderate to intense	Moderate to intense
Location (S; W)	32°25′52″ 69°06′34″	32°25′51″ 69°06′34″	32°25′56″ 69°06′28″	32°25′56″ 69°06′28″	32°25′ 40,5″ 69°05′59,5″	32°25′01,9″ 69°06′05,2″	32 25′48,4″ 69 06′03,3″	32°25′48,4′ 69°06′03,3″	32°26′09,1″ 69°06′07,5″	32°27′35″ 69°06′49″	32°27′36″ 69°06′49″	32°27′53″ 69°06′40″	32°27′53″ 69°06′40″	32°27′53″ 69°06′40″	32°27′53″ 69°06′40″	32°30′33″ 69°07′05″	32°29′54″ 69°06′54″
SiO_2	61.76	59.63	60.10	59.28	59.83	55.18	61.31	60.19	59.20	56.73	57.19	64.30	63.94	63.35	63.72	59.95	60.07
TiO_2	0.65	0.66	0.63	0.50	0.55	0.55	0.45	0.43	0.67	0.76	0.83	0.53	0.52	0.52	0.58	1.09	1.19
Al_2O_3	18.00	17.13	19.69	17.04	18.30	18.82	18.02	17.87	19.97	19.04	20.75	17.72	17.47	17.69	17.48	20.62	20.56
$Fe_2O_3^t$	3.33	5.54	3.21	1.26	4.33	7.79	3.63	3.41	4.91	6.14	2.38	3.85	4.11	4.47	2.98	2.31	1.73
MnO	0.01	0.00	0.01	0.07	0.11	0.08	0.12	0.10	0.11	0.17	0.07	0.01	0.13	0.12	0.08	0.00	0.01
MgO	0.27	0.39	0.57	0.13	0.68	0.63	0.50	0.64	0.68	1.37	1.16	0.94	0.81	0.83	1.31	0.53	0.96
CaO	0.30	0.75	0.45	5.55	3.85	1.76	4.04	3.60	5.58	7.28	8.96	5.39	4.84	4.75	6.03	1.00	1.08
Na_2O	2.97	6.57	3.66	6.75	4.84	4.59	4.82	5.62	4.82	4.50	6.06	5.28	4.75	4.75	6.19	5.31	5.11
K_2O	9.81	3.13	8.09	4.49	5.48	6.09	4.82	4.83	3.98	3.64	0.39	2.37	3.16	3.27	1.06	4.33	4.92
P_2O_5	0.11	0.24	0.14	0.11	0.20	0.11	0.13	0.15	0.26	0.30	0.41	0.20	0.16	0.16	0.24	0.12	0.12
LOI	2.59	5.94	2.81	4.79	1.51	3.03	0.68	1.61	0.74	0.23	1.47	0.64	0.46	0.45	0.96	3.33	2.38
Total	99.81	99.98	99.36	99.98	99.68	98.62	98.52	98.46	100.90	100.15	99.69	100.65	100.33	100.36	100.52	98.59	98.13
Rb	393.00	154.00	422.00	142.00	170.00	161.00	145.00	131.00	131.00	112.00	16.00	81.00	112.00	118.00	51.00	173.00	193.00
Sr	611.00	561.00	550.00	360.00	1214.00	978.00	1267.00	1018.00	1514.00	1560.00	1688.00	1031.00	915.00	996.00	1218.00	740.00	884.00
Y	21.00	24.00	15.00	26.00	24.00	21.00	23.00	23.00	27.00	40.00	37.00	25.00	27.00	25.00	24.00	6.00	12.00
Zr	342.00	207.00	334.00	302.00	208.00	290.00	219.00	171.00	163.00	151.00	127.00	194.00	205.00	207.00	169.00	166.00	180.00
Nb	15.00	11.00	14.00	15.00	9.00	20.00	11.00	9.00	9.00	3.00	0.90	5.00	7.00	6.00	7.00	–	–
Cs	–	2.00	4.00	0.90	1.10	2.60	1.00	1.00	1.00	–	–	1.00	2.00	2.00	0.90	–	–
Ba	1782.00	720.00	1142.00	864.00	1024.00	1860.00	925.00	837.00	825.00	1170.00	229.00	656.00	946.00	901.00	342.00	404.00	501.00
Hf	9.00	7.00	10.00	10.00	5.00	5.80	5.20	4.40	4.10	6.00	5.00	4.00	4.00	6.00	4.00	3.00	3.00
Ta	–	–	–	–	0.60	0.90	0.70	0.60	0.70	–	–	–	–	–	–	–	–
Th	10.00	9.00	7.00	12.00	5.70	12.40	6.20	5.60	5.90	–	–	–	5.00	–	–	0.90	0.90
U	3.00	3.00	4.00	3.00	2.70	6.70	2.60	2.20	2.20	1.90	1.90	1.90	1.90	1.90	1.90	1.90	3.00
Sc	3.00	5.00	2.00	9.00	3.00	3.00	2.00	3.00	5.00	7.00	12.00	9.00	10.00	6.00	7.00	4.90	13.00
V	84.00	109.00	66.00	40.00	74.00	89.00	47.00	44.00	99.00	85.00	98.00	41.00	32.00	32.00	55.00	84.00	79.00
Cr	30.00	29.00	18.00	54.00	–	–	–	–	–	54.00	72.00	72.00	29.00	77.00	67.00	2.90	2.90
Ni	1.90	1.90	3.00	3.00	–	–	–	–	–	1.70	1.90	1.90	1.90	1.90	1.90	1.90	1.90
Co	1.90	3.00	1.90	6.00	16.00	14.00	22.00	18.00	21.00	10.00	4.00	1.90	34.00	1.90	3.00	12.00	11.00
Ga	21.00	23.00	22.00	19.00	21.00	24.00	21.00	20.00	22.00	17.00	20.00	17.00	18.00	18.00	19.00	19.00	20.00
La	68.00	12.00	49.00	26.00	37.20	40.00	37.70	30.00	37.10	47.00	37.00	23.00	35.00	29.00	15.00	39.00	65.00
Ce	60.00	32.00	81.00	36.00	76.90	76.50	77.60	68.10	75.70	78.00	85.00	65.00	42.00	57.00	34.00	64.00	126.00
Pr	–	–	–	–	9.24	8.71	9.09	8.41	9.66	–	–	–	–	–	–	–	–
Nd	31.00	21.00	40.00	21.00	36.30	34.20	36.40	33.30	40.20	50.00	55.00	30.00	25.00	27.00	17.00	29.00	69.00
Sm	–	6.30	4.10	3.30	7.70	6.80	7.00	7.00	8.20	–	–	5.70	6.00	5.80	5.20	6.40	7.50
Eu	–	1.80	1.40	1.00	2.07	2.50	1.93	1.78	2.39	–	–	1.80	2.00	1.90	1.60	1.60	1.70
Gd	–				5.90	5.70	5.40	5.10	6.80	–	–	–	–	–	–	–	–
Tb	–	0.90	0.60	0.49	0.90	0.80	0.80	0.80	0.90	–	–	0.49	0.70	0.70	0.60	0.90	0.90
Dy	–	–	–	–	4.50	3.90	4.20	4.00	4.60	–	–	–	–	–	–	–	–
Ho	–	–	–	–	0.90	0.70	0.80	0.80	0.90	–	–	–	–	–	–	–	–
Er	–	–	–	–	2.60	2.20	2.60	2.40	2.70	–	–	–	–	–	–	–	–
Tm	–	–	–	–	0.39	0.32	0.37	0.35	0.40	–	–	–	–	–	–	–	–
Yb	–	2.40	4.00	3.30	2.80	2.30	2.70	2.40	2.70	–	–	2.60	2.50	2.50	2.10	1.00	1.90
Lu	–	0.33	0.60	0.48	0.47	0.37	0.48	0.42	0.46	–	–	0.37	0.36	0.37	0.29	0.20	0.30
Sm/Yb	–	2.63	1.03	1.00	2.75	2.96	2.59	2.92	3.04	–	–	2.19	2.40	2.32	2.48	6.40	3.95
La/Sm	–	1.90	11.95	7.88	4.83	5.88	5.39	4.29	4.52	–	–	4.04	5.83	5.00	2.88	6.09	8.67
La/Yb	–	5.00	12.25	7.88	13.29	17.39	13.96	12.50	13.74	–	–	8.85	14.00	11.60	7.14	39.00	34.21
Eu/Eu*	–	0.94	1.22	1.07	0.94	1.23	0.96	0.91	0.98	–	–	1.44	1.25	1.21	1.16	0.76	0.80
Ba/La	26.21	60.00	23.31	33.23	27.53	46.50	24.54	27.90	22.24	24.89	6.19	28.52	27.03	31.07	22.80	10.36	7.71

Please cite this article in press as: Carrasquero, S.I., et al., New insights into petrogenesis of Miocene magmatism associated with porphyry copper deposits of the Andean Pampean flat slab, Argentina, Geoscience Frontiers (2017), https://doi.org/10.1016/j.gsf.2017.10.009

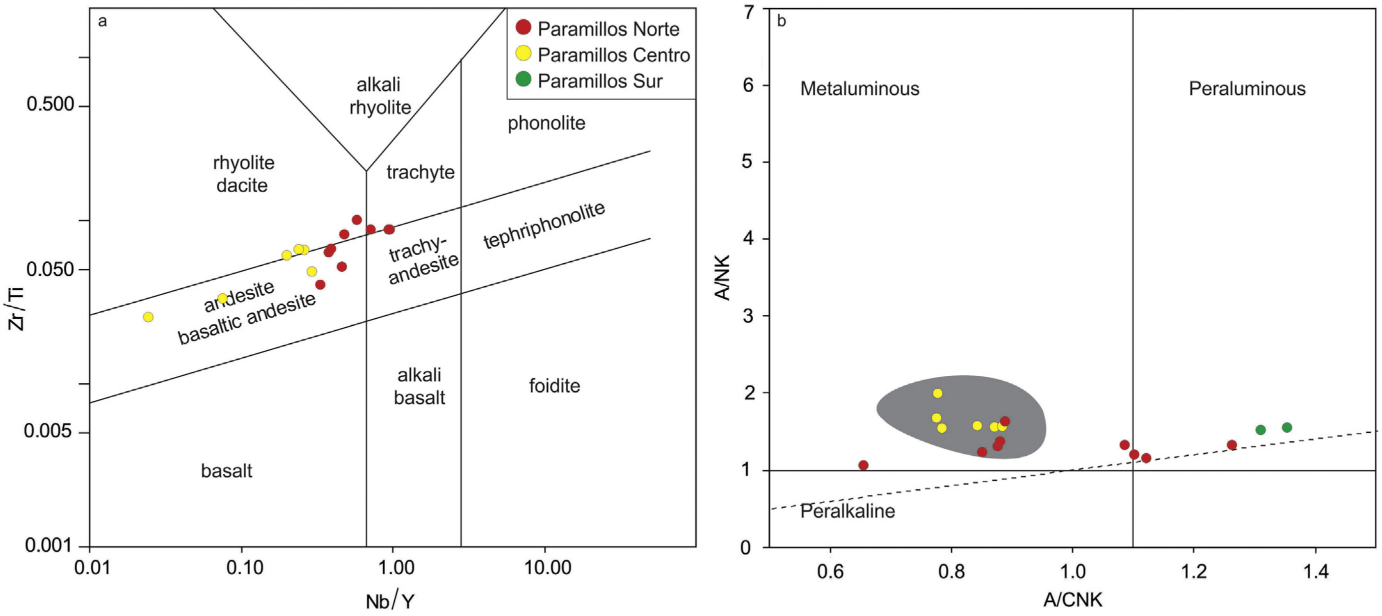

Figure 4. (a) Nb/Y vs. Zr/TiO$_2$ classification diagram (Pearce, 1996); (b) aluminum saturation index diagram (A/CNK; Shand, 1943). The gray field corresponds to Miocene unaltered rocks of Precordillera from Kay et al. (1991) and Cortés et al. (1997).

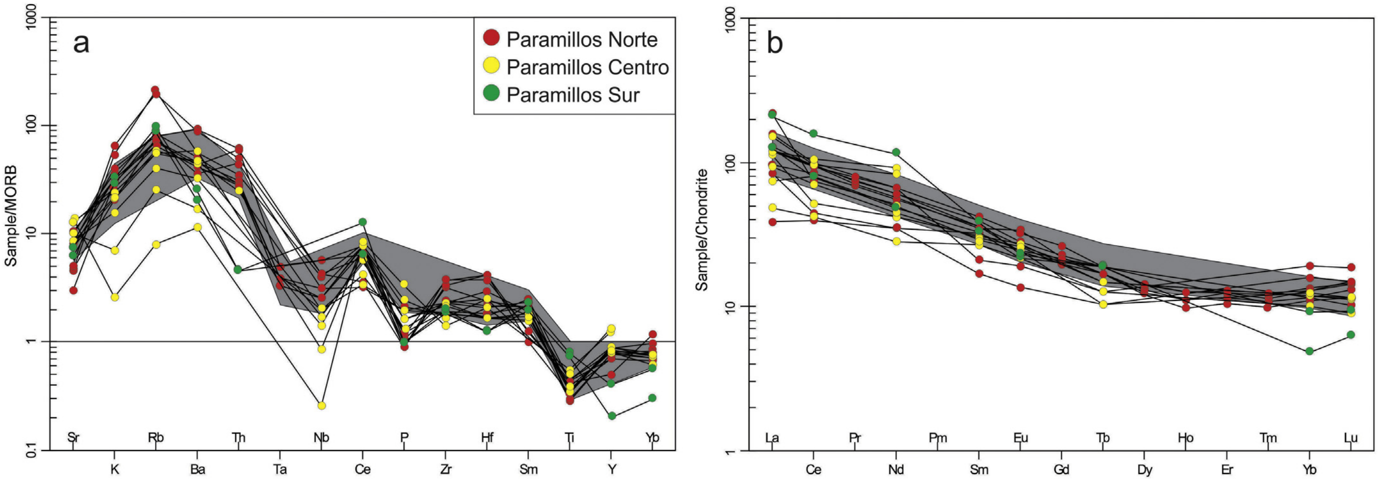

Figure 5. (a) Spider diagram normalized to MORB (Pearce, 1983); (b) REE diagram normalized to chondrite (Boynton, 1984). The gray field corresponds to Miocene unaltered rocks of Precordillera from Kay et al. (1991) and Cortés et al. (1997).

(Tosdal and Richards, 2001; Billa et al., 2004; Japas et al., 2013). These geodynamic conditions were particularly observed in the middle Eocene to early Oligocene and a Miocene to early Pliocene belts of the Central Andes where porphyry type deposits developed in a slab shallowing setting (Sillitoe and Perelló, 2005). Despite the lack of stratigraphics evidences (Ramos et al., 2002), the broadening of the Farellones arc and a residual mineralogy typical of relative deep magmatic chambers that we recorded in the Paramillos area, are consistent with a slab shallowing and outcoming crustal thickening conditions, which could be the result of an early effect of the JFR collision that was further to the north by ~17 Ma. Besides, our isotopic values reflect MASH processes occurring in these chambers, typical of this tectonic scenario. In this way, the contribution of MASH processes in the acquisition of the adakitic signal cannot be disregarded.

Albeit major porphyry deposits of Miocene to early Pliocene of the Central Andes are ≤15 Ma and linked to the peak of the slab shallowing (see Kay and Mpodozis, 2002; Bissig et al., 2003 and a comprehensive review in; Sillitoe and Perelló, 2005), our results reveal that even during the early stages of the slab shallowing the magmas were fertile although not necessarily gave rise to major deposits. If this is so, it can be argued that although JFR subduction may have played a role in slab flattening, it seems to have no direct relationship with porphyry deposits generation as it was previously noted by Deckart et al. (2005) and Sillitoe and Perelló (2005).

7. Concluding remarks

This paper provides a possible petrogenetic model for the magmatism precursor of porphyry type deposits located in the

Please cite this article in press as: Carrasquero, S.I., et al., New insights into petrogenesis of Miocene magmatism associated with porphyry copper deposits of the Andean Pampean flat slab, Argentina, Geoscience Frontiers (2017), https://doi.org/10.1016/j.gsf.2017.10.009

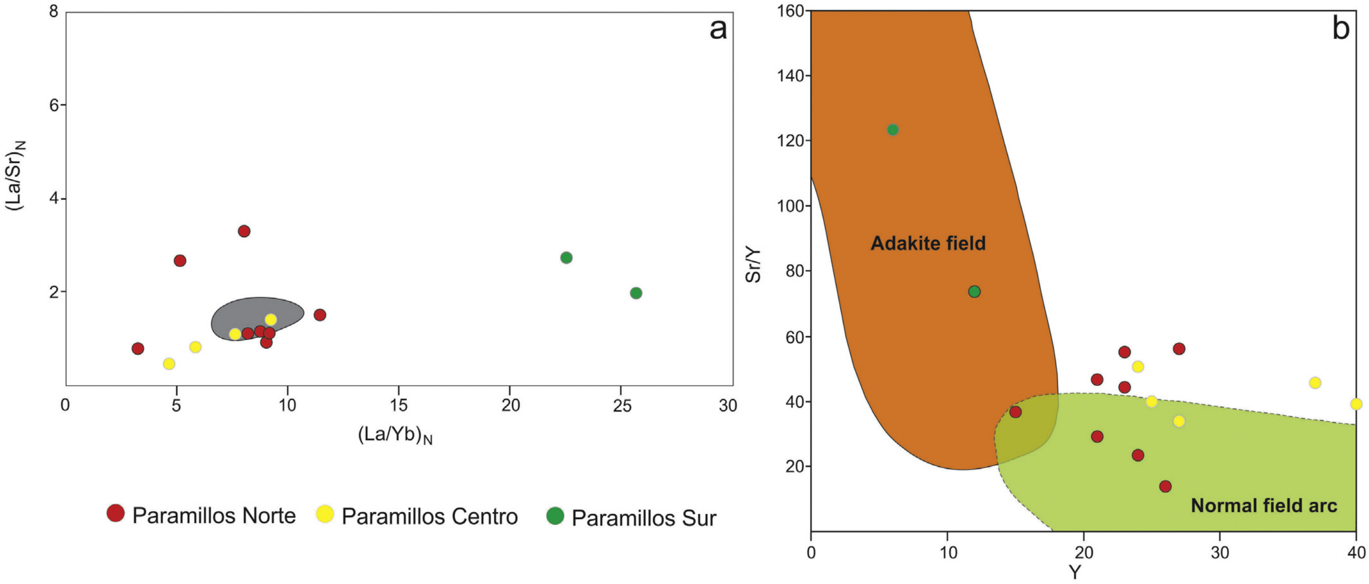

Figure 6. (a) $(La/Sr)_N$ vs. $(La/Yb)_N$. The gray field corresponds to Miocene unaltered rocks of Precordillera from Kay et al. (1991) and Cortés et al. (1997). Normalization values according to Kay et al. (1991); (b) Sr/Y vs. Y diagram (Castillo et al., 1999) discriminating normal arc magmas from adakitic-like magmas. The samples that plot above the normal arc field have high Sr/Y ratios as a result of sodic-calcic alteration (see Table 2).

Table 3
Whole-rocks Nd, Sr and Pb isotopic ratios of Miocene volcanics from the study area.

Sample	UP82	UP84	UP85	UP69	GN14
Sm (ppm)	6.3	4.1	3.3	5.7	6.4
Nd (ppm)	21	84	21	30	29
$^{143}Sm/^{144}Nd$	0.1806	0.0294	0.0946	0.1144	0.1329
$(^{143}Nd/^{144}Nd)_m$	0.5128	0.5128	0.5126	0.5125	0.5126
2σ	0.000008	0.000006	0.000011	0.000006	0.000009
$(^{143}Nd/^{144}Nd)_T$	0.5128	0.5128	0.5126	0.5125	0.5126
ε_{Nd}	2.88	2.96	−0.62	−1.98	−1.05
Sr (ppm)	561	550	360	1031	740
Rb (ppm)	154	422	142	81	173
$^{87}Rb/^{86}Sr$	0.794	2.219	1.141	0.267164	0.676
$(^{87}Sr/^{86}Sr)_m$	0.7045	0.7045	0.7047	0.7054	0.7058
2σ	0.000006	0.000012	0.000003	0.000003	0.000002
$(^{87}Sr/^{86}Sr)_T$	0.7043	0.7040	0.7045	0.7053	0.7056
$^{206}Pb/^{204}Pb$	18.7841	18.6976	18.7384	18.4732	18.5178
Std error	0.0008	0.0006	0.0016	0.0004	0.0004
$^{207}Pb/^{204}Pb$	15.6309	15.6118	15.6145	15.5865	15.5868
Std error	0.0008	0.0006	0.0015	0.0004	0.0003
$^{208}Pb/^{204}Pb$	38.5662	38.4616	38.5403	38.2557	38.3091
Std error	0.0023	0.0014	0.0035	0.001	0.0008

backarc of the Pampean flat-slab which has been poorly analyzed so far.

Our new petrological data confirm the association between the porphyry type deposits of the Paramillos region with the Middle Miocene magmatism which has a typical arc signature suggesting the broadening of the Farellones arc by ~17 Ma. These mineralizing magmas, formed in relatively deep chambers, show an adakitic signal typical of fertile magmas, resulting from amphibole ± garnet fractionation and probably also the contribution of MASH processes.

Despite the lack of any stratigraphics evidence, both the broadening of the Farellones arc and the petrological feature of the Paramillos magmatism are consistent with a slab shallowing and outcoming crustal thickening conditions, which could be the result of an early effect of the JFR collision that was further to the north by ~17 Ma. In this context, we consider that magmas were fertile for porphyry type deposits during the early stages of the slab shallowing.

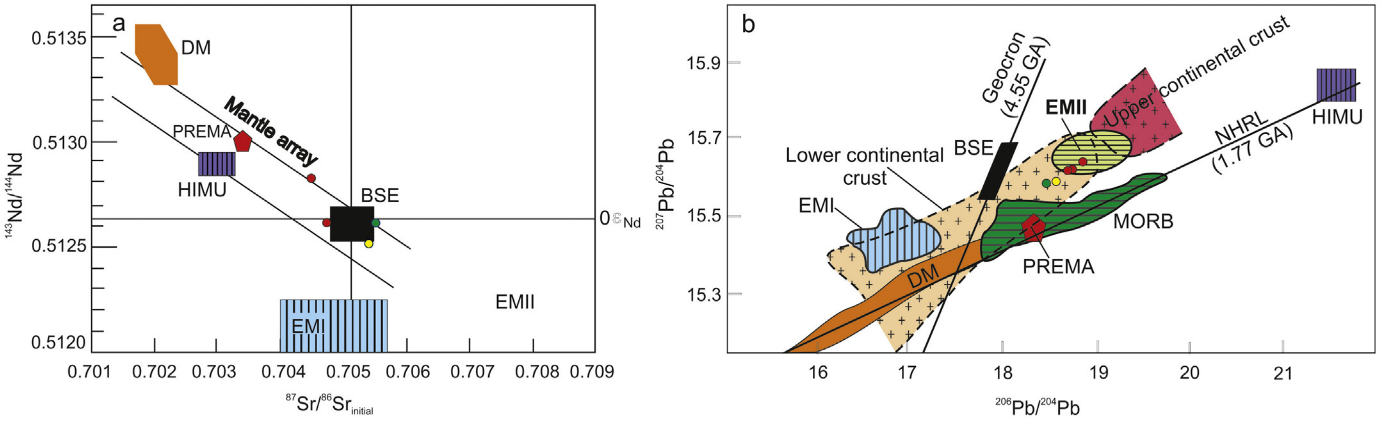

Figure 7. Isotope correlation diagrams from Rollinson (1995): (a) $^{143}Nd/^{144}Nd$ versus $^{87}Sr/^{86}Sr$ diagram. The mantle array is defined by many oceanic basalts and bulk earth value for $^{87}Sr/^{86}Sr$ can be obtained from this trend; (b) $^{207}Pb/^{204}Pb$ versus $^{206}Pb/^{204}Pb$ diagram showing the position of the northern hemisphere reference line (NHRL). Mantle reservoirs of Zindler and Hart (1986): DM—depleted mantle; BE—bulk silicate Earth; EMI, EMII—enriched mantle; HIMU—mantle with high U/Pb ratio; PREMA—PREvalent Mantle composition.

Please cite this article in press as: Carrasquero, S.I., et al., New insights into petrogenesis of Miocene magmatism associated with porphyry copper deposits of the Andean Pampean flat slab, Argentina, Geoscience Frontiers (2017), https://doi.org/10.1016/j.gsf.2017.10.009

Acknowledgments

The authors wish to thank the Servicio Geológico Minero Argentino (SEGEMAR) for their support during the fieldwork. This research was funded by Universidad de Buenos Aires (UBA-CyT 20020090100182) and FonCyT, Argentina (PICT-2014-1280). Constructive comments by anonymous reviewers helped eliminate inconsistencies and improve the clarity of this paper.

References

Alonso-Perez, R., Muntener, O., Ulmer, P., 2009. Igneous garnet and amphibole fractionation in the roots of island arcs: experimental constraints on H_2O undersaturated andesitic liquids. Contributions to Mineralogy and Petrology 157, 541–558.

Atherton, M.P., Petford, N., 1993. Generation of sodium-rich magmas from newly underplated basaltic crust. Nature 362, 144–146.

Barazangi, M., Isacks, B.I., 1976. Spatial distribution of earthquakes and subduction of the Nazca Plate beneath South America. Geology 4, 686–692.

Barredo, S., Chemale, F., Marsicano, C., Ávila, J.N., Ottone, E.G., Ramos, V.A., 2012. Tectono-sequence stratigraphy and U–Pb zircon ages of the Rincón Blanco Depocenter, northern Cuyo Rift, Argentina. Gondwana Research 21, 264–631.

Billa, M., Cassard, D., Lips, A.L.W., Bouchot, V., Tourlière, B., Stein, G., Guillou-Frottier, L., 2004. Predicting gold-rich epithermal and porphyry systems in the Central Andes with a continental-scale metallogenic GIS. Ore Geology Reviews 25, 39–67.

Bissig, T., Clark, A., Von Quadt, A., 2003. Petrogenetic and metallogenetic responses to Miocene slab flattening: new constraints from the El Indio-Pascua Au-Ag-Cu belt, Chile/Argentina. Mineralium Deposita 38, 844–862.

Boynton, W.V., 1984. Cosmochemistry of the rare-earth elements: meteorite studies. In: Henderson, P. (Ed.), Rare Earth Element Geochemistry. Elsevier Science Publications Co., Amsterdam, Nederland, pp. 63–114.

Castillo, P., Janney, P., Solidum, R., 1999. Petrology and geochemistry of Camiguin Island, southern Philippines: insights to the source of adakites and other lavas in a complex arc setting. Contributions to Mineralogy and Petrology 134, 33–51.

Chang, Z., Vervoort, J.D., McClelland, W.C., Knaack, C., 2006. U-Pb dating of zircon by LAICP-MS. Geochemistry, Geophysics, Geosystems 7, 1–14.

Chiaradia, M., 2015. Crustal thickness control on Sr/Y signatures of recent arc magmas: an Earth scale perspective. Scientific Reports 5. https://doi.org/10.1038/srep08115. Article number: 8115.

Chiaradia, M., Ulianov, A., Kouzmanov, K., Beate, B., 2012. Why large porphyry Cu deposits like high Sr/Y magmas? Scientific Reports 2. https://doi.org/10.1038/srep00685. Article number: 685.

Cline, J.S., Bodnar, R.J., 1991. Can economic porphyry copper mineralization be generated by a typical calc-alkaline melt? Journal of Geophysical Research 96, 8113–8126.

Cortés, J.M., González Bonorino, M., Koukharsky, M., Pereyra, F.X., Brodkorb, A., 1997. Hoja 3369-09, Uspallata. Servicio Geológico Minero Argentino, Buenos Aires, Argentina, p. 165.

Deckart, K., Clark, A.H., Aguilar, C., Vargas, R., Bertens, A., Mortensen, J.K., Fanning, M., 2005. Magmatic and hydrothermal chronology of the giant Río Blanco porphyry copper deposit, Central Chile: implications of an integrated U/Pb and $^{40}Ar/^{39}Ar$ database. Economic Geology 100, 905–934.

Defant, M.J., Drummond, M.S., 1990. Derivation of some modern arc magmas by melting of young subducted lithosphere. Nature 347, 662–665.

Defant, M.J., Xu, J.F., Kepezhinkas, P., Wang, Q., Zhang, Q., Xiao, O.L., 2002. Adakites: some variations on a theme. Acta Petrologica Sinica 18, 129–142.

Harrington, H., 1971. Hoja Geológica 22c, Ramblón. Dirección de Minería de la Nación, Buenos Aires, Argentina, p. 89.

Hildreth, W., Moorbath, S., 1988. Crustal contributions to arc magmatism in the Andes of Central Chile. Contributions to Mineralogy and Petrology 98, 455–489.

Hoffman, E.L., 1992. Instrumental neutron activation in geoanalysis. Journal of Geochemical Exploration 44, 297–319.

Japas, M.S., Rubinstein, N.A., Kleiman, L.E., 2013. Strain fabric analysis applied to hydrothermal ore deposits emplaced during changing geodynamical conditions (Infiernillo and Las Picazas, San Rafael Massif, Argentina). Ore Geology Reviews 53, 357–372.

Jordan, T.E., Isacks, B.L., Almendinger, R.W., Brewer, J.A., Ramos, V.A., Ando, C.J., 1983. Andean tectonics related to geometry of subducted Nazca plate. Geological Society of America Bulletin 94, 341–361.

Kay, S.M., Mpodozis, C., 2002. Magmatism as a probe to the Neogene shallowing of the Nazca plate beneath the modern Chilean flat-slab. Journal of South American Earth Sciences 15, 39–57.

Kay, S.M., Maksaev, V., Moscoso, R., Mpodozis, C., Nasi, C., 1987. Probing the evolving Andean lithosphere: Mid-late Tertiary magmatism in Chile (29°–30°30′S) over the modern zone of sub-horizontal subduction. Journal of Geophysical Research 92, 6173–6189.

Kay, S.M., Mpodozis, C., Ramos, V., Munizaga, F., 1991. Magma source variations for mid-late Tertiary magmatics rocks associated with a shallowing subduction zone and a thickening crust in the central Andes (28° to 33°S). In: Harmon, R., Rapela, C.W. (Eds.), Andean Magmatism and its Tectonic Setting, Special Paper 265. Geological Society of America, Boulder, Colorado, US, pp. 113–137.

Kay, S.M., Godoy, E., Kurtz, A., 2005. Episodic arc migration, crustal thickening, subduction erosion, and magmatism in the south-central Andes. Geological Society of America Bulletin 117, 67–88.

Kay, S.M., Burns, W.M., Copeland, P., Mancilla, O., 2006. Upper Cretaceous to Holocene magmatism and evidence for transient Miocene shallowing of the Andean subduction zone under the northern Neuquén Basin. In: Kay, S.M., Ramos, V.A. (Eds.), Late Cretaceous to Recent Magmatism and Tectonism of the Southern Andean Margin at the Latitude of the Neuquén Basin (36°–39°S), Special Paper 407. Geological Society of America, Boulder, Colorado, US, pp. 19–60.

Kleiman, L.E., Japas, M.S., 2009. The Choiyoi volcanic province at 34°S–36°S (San Rafael, Mendoza, Argentina): implications for the late Palaeozoic evolution of the southwestern margin of Gondwana. Tectonophysics 473, 283–299.

Koukharsky, M., Munizaga, F., Brodtkorb, A., 1998. Nuevas edades K-Ar de las rocas alteradas de Paramillos Sur y Norte. Interpretación de los resultados. In: Proc. 10° Congreso Latinoamericano de Geología y 6° Congreso Nacional de Geología Económica, vol. 3, pp. 220–225. Buenos Aires, Argentina.

Lavandaio, E., Fusari, C., 1999. Distrito polimetálico Mendoza Norte, Mendoza. In: Zappettini, E. (Ed.), Recursos Minerales de la República Argentina. Servicio Geológico Minero Argentino (SEGEMAR), Buenos Aires, Argentina, pp. 1705–1716.

Legarreta, L., Uliana, M.A., 1996. The Jurassic succession in west central Argentina: stratal pattern, sequences and paleogeographic evolution. Palaeogeography, Palaeoclimatology, Palaeoecology 120, 303–330.

López Escobar, E., 1982. Características geoquímicas de rocas ígneas asociadas con pórfidos cupríferos chilenos. Revista Geológica de Chile 17, 3–19.

Loucks, R.R., 2014. Distinctive composition of copper-ore-forming arc magmas. Australian Journal of Earth Sciences 61, 5–16.

Ludwig, K.R., 2003. Isoplot 3.0-Ageochronological Toolkit for Microsoft Excel, Special Publication 4. Berkeley Geochronology Center, Berkeley, California, US, p. 71.

Martin, H., 1999. Adakitic magmas: modern analogues of Archaean granitoids. Lithos 46, 411–429.

Massabie, A.H., 1986. Filón-capa Paramillos de Uspallata, su caracterización geológica y edad, Paramillos de Uspallata, Mendoza. In: Proc. 1° Jornadas sobre Geología de Precordillera, San Juan, Argentina, pp. 325–330.

Massabie, A.H., Rapalini, A., Soto, J.L., 1986. Estratigrafía del Cerro Los Colorados, Paramillos de Uspallata, Mendoza. In: Proc. 1° Jornadas sobre Geología de Precordillera, San Juan, Argentina, pp. 71–76.

Muntener, O., Kelemen, P.B., Grove, T.L., 2001. The role of H_2O during crystallization of primitive arc magmas under uppermost mantle conditions and genesis of igneous pyroxenites: an experimental study. Contributions to Mineralogy and Petrology 141, 643–658.

Oyarzún, R., Márquez, A., Lilo, J., López, L., Rivera, S., 2001. Giant versus small porphyry copper deposits of Cenozoic age in northern Chile: adakitic versus normal calc-alkaline magmatism: Reply. Mineralium Deposita 37, 795–799.

Paces, J.B., Miller, J.D., 1993. Precise U-Pb ages of Duluth complex and related mafic intrusions, northeastern Minnesota; geochronological insights to physical, petrogenetic, paleomagnetic, and tectonomagmatic processes associated with the 1.1 Ga midcontinent rift system. Journal of Geophysical Research 98 (B8), 13997–14013.

Peacock, S.M., Rushmer, T., Thompson, A.B., 1994. Partial melting of subducting oceanic crust. Earth and Planetary Sciences Letters 121, 227–244.

Pearce, J.A., 1983. Role of the sub-continental lithosphere in magma genesis at active continental margins. In: Hawkesworth, C.J., Norry, M.J. (Eds.), Continental Basalts and Mantle Xenoliths. Shiva Publication, Nantwich, Cheshire, UK, pp. 230–249.

Pearce, J.A., 1996. A users guide to basalt discrimination diagrams. In: Wyman, D.A. (Ed.), Trace Element Geochemistry of Volcanic Rocks: Applications for Massive Sulphide Exploration, Short Course Notes, 12. Geological Association of Canada, Canada, 79–113.

Petford, N., Atherton, M., 1996. Na-rich partial melts from newly underplated basaltic crust: the Cordillera Blanca Batholith, Peru. Journal of Petrology 37, 1491–1521.

Rabbia, O., Hernandez, L., King, R.W., López-Escobar, L., 2002. Giant versus small porphyry copper deposits of Cenozoic age in northern Chile: adakitic versus normal calc-alkaline magmatism: Discussion. Mineralium Deposita 36, 794–798.

Ramos, V., Kay, S.M., 1991. Triassic rifting and associated basalts in the Cuyo basin, central Argentina. In: Harmon, R., Rapela, C.W. (Eds.), Andean Magmatism and its Tectonic Setting, Special Paper 265. Geological Society of America, Boulder, Colorado, pp. 79–91.

Ramos, V., Jordan, T.E., Allmendinger, R.W., Mpodozis, C., Kay, S.M., Cortés, J.M., Palma, M.A., 1986. Paleozoic terranes of the central Argentine Chilean Andes. Tectonics 5, 8555–8880.

Ramos, V., Cristallini, E.O., Pérez, D., 2002. The Pampean flat-slab on the central Andean. South American Earth Sciences 15, 59–78.

Reich, M., Parada, M., Palacios, C., Dietrich, A., Schultz, F., Lehmann, B., 2003. Adakite-like signature of Late Miocene Intrusions at the Los Pelambres giant porphyry copper deposit in the Andes of central Chile: metallogenic implications. Mineralium Deposita 38, 876–885.

Richards, J.P., 2003. Tectono-magmatic precursors for porphyry Cu–(Mo–Au) deposit formation. Economic Geology 98, 1515–1533.

Richards, J.P., 2011. Magmatic to hydrothermal metal flux in convergent and collided margins. Ore Geology Review 40, 1–26.

Please cite this article in press as: Carrasquero, S.I., et al., New insights into petrogenesis of Miocene magmatism associated with porphyry copper deposits of the Andean Pampean flat slab, Argentina, Geoscience Frontiers (2017), https://doi.org/10.1016/j.gsf.2017.10.009

Richards, J.P., Kerrich, R., 2007. Adakite-like rocks: their diverse origins and questionable role in metallogenesis. Economic Geology 102, 537–576.

Rivano, S., Godoy, E., Vergara, M., Villaroel, R., 1990. Redefinición de la Formación Farellones en la Cordillera de los Andes de Chile Central (32°–34°S). Revista Geológica de Chile 17, 205–214.

Rollinson, H.R., 1995. Using Geochemical Data: Evaluation, Presentation, Interpretation. Longman Scientific and Technical, Harlow, Essex, UK, p. 352.

Romani, R.R., 1999. El pórfiro cuprífero Paramillos Sur, Mendoza. In: Zappettini, E. (Ed.), Recursos Minerales de la República Argentina. Servicio Geológico Minero Argentino (SEGEMAR), Buenos Aires, Argentina, pp. 1705–1716.

Rubatto, D., 2002. Zircon trace element geochemistry: distribution coefficients and the link between U-Pb ages and metamorphism. Chemical Geology 184, 123–138.

Shand, S.J., 1943. Eruptive Rocks. Their Genesis, Composition, Classification, and Their Relation to Ore-Deposits with a Chapter on Meteorite. John Wiley & Sons, New York, p. 444.

Sillitoe, R., 1977. Permo-carboniferous, Upper Cretaceous, and Miocene porphyry copper-type mineralization in the Argentinian Andes. Economic Geology 72, 99–109.

Sillitoe, R., 2010. Porphyry copper systems. Economic Geology 105, 3–41.

Sillitoe, R., Perelló, J., 2005. Andean Copper Province: tectonomagmatic settings, deposit types, metallogeny, exploration, and discovery. Economic Geology 100th Anniversary Volume, 845–890.

Sláma, J., Košler, J., Condon, D.J., Crowley, J.L., Gerdes, A., Hanchar, J.M., Horstwood, M.S.A., Morris, G.A., Nasdala, L., Norberg, N., Schaltegger, U., Schoene, B., Tubrett, M.N., Whitehouse Plešovice, M.J., 2008. Zircon, a new natural reference material for U-Pb and Hf isotopic microanalysis. Chemical Geology 249, 1–35.

Spalletti, L.A., 1999. Cuencas triásicas del Oeste argentino: origen y evolución. Acta Geológica Hispánica 32, 29–50.

Spalletti, L.A., Fanning, C.M., Rapela, C.W., 2008. Dating the Triassic continental rift in the southern Andes: the Potrerillos Formation, Cuyo Basin, Argentina. Geologica Acta 6, 267–283.

Tanaka, T., Togashi, S., Kamiokab, H., Amakawa, H., Kagami, H., Hamamoto, T., Yuhara, M., Orihashi, Y., Yonedaf, S., Shimizu, H., Kunimaru, T., Takahashi, K., Yanagi, T., Nakano, T., Fujimaki, H., Shinjo, R., Asaharaa, Y., Tanimizu, M., Dragusanu, C., 2000. JNdi-1: a neodymium isotopic reference in consistency with La Jolla neodymium. Chemical Geology 168, 279–281.

Thiéblemont, D., Stein, G., Lescuyer, J.L., 1997. Epithermal and porphyry deposits: the adakite connexion. Comptes Rendus de l'Académie des Sciences Series A 325, 103–109.

Todt, W., Cliff, R.A., Hanser, A., Hofmann, A.W., 1984. ^{202}Pb-^{205}Pb spike for Pb isotopic analysis. Terra Cognita 4, 209.

Tosdal, R.M., Richards, J.P., 2001. Magmatic and structural controls on the development of porphyry Cu ± Mo ± Au deposits. In: Richards, J.P., Tosdal, R.M. (Eds.), Structural Controls on Ore Deposits, Reviews in Economic Geology, vol. 14. Society of Economic Geologists Inc., Boulder, Colorado, US, pp. 157–181.

Valencia, V.A., Ruiz, J., Barra, F., Gehrels, G., Ducea, M., Titley, S.R., Ochoa-Landín, L., 2005. U/Pb zircon and Re/Os molybdenite geochronology from La Caridad porphyry copper deposit—insights for the duration of magmatism and mineralization in the Nacozari District, Sonora, Mexico. Mineralium Deposita 40, 175–191.

Xu, J.F., Shinjo, R., Defant, M.J., Wang, Q., Rapp, R.P., 2002. Origin of Mesozoic adakitic intrusive rocks in the Ningzhen area of east China: partial melting of delaminated lower continental crust? Geology 30, 1111–1114.

Yáñez, G., Ranero, C., Von Huene, R., Díaz, J., 2001. Magnetic anomaly interpretation across the southern central Andes (32°–34°S): the role of the Juan Fernandez Ridge in the late Tertiary evolution of the margin. Journal of Geophysical Research 106 (B4), 6325–6345.

Yogodzinski, G.M., Lees, J.M., Churikova, T.G., Dorendorf, F., Woerner, G., Volynets, O.N., 2001. Geochemical evidence for the melting of subducting oceanic lithosphere at plate edges. Nature 409, 500–504.

Zindler, A., Hart, S., 1986. Chemical geodynamics. Annual Review Earth and Planetary Sciences 14, 493–571.

Please cite this article in press as: Carrasquero, S.I., et al., New insights into petrogenesis of Miocene magmatism associated with porphyry copper deposits of the Andean Pampean flat slab, Argentina, Geoscience Frontiers (2017), https://doi.org/10.1016/j.gsf.2017.10.009